

Article

Elimination of Chromium (VI) and Nickel (II) Ions in a Packed Column Using Oil Palm Bagasse and Yam Peels

Angel Villabona-Ortiz ¹, Candelaria Tejada-Tovar ^{1,*} and Ángel Darío González-Delgado ^{2,*}

¹ Process Design and Biomass Utilization Research Group (IDAB), Chemical Engineering Department, Universidad de Cartagena, Avenida del Consulado St. 30, Cartagena de Indias 130015, Colombia; avillabona@unicartagena.edu.co

² Nanomaterials and Computer Aided Process Engineering Research Group (NIPAC), Chemical Engineering Department, Universidad de Cartagena, Avenida del Consulado St. 30, Cartagena de Indias 130015, Colombia

* Correspondence: ctejadat@unicartagena.edu.co (C.T.-T.); agonzalezd1@unicartagena.edu.co (Á.D.G.-D.)

Abstract: The single-component adsorption of chromium (VI) and nickel (II) on oil palm bagasse (OPB) and yam peels (YP) in a packed bed column was explored and improved using a central 2²-star T composite design. The temperature, bed height, and particle size were evaluated, and the optimized response variable was the removal efficiency. The remaining concentration of heavy metals in solution was determined by Ultraviolet-Visible and Atomic Absorption Spectroscopy. It was found that bioadsorbents have a porous structure, with the presence of functional groups such as hydroxyl, carboxyl, and amino, which favor adsorption processes, and that the adsorption mechanisms controlling the process is cation exchange, precipitation, and complexation on the exposed surface of the biomaterials. In the adsorption trials, removal percentages higher than 87% were obtained in all cases, showing better results in the removal of Cr(VI), and that particle size is the most influential factor. Maximum Cr(VI) capacities of 111.45 mg g⁻¹ and 50.12 mg g⁻¹ were achieved on OPB and YP, respectively, while for nickel values of 103.49 mg g⁻¹ and 30.04 mg g⁻¹ were obtained. From the adjustment of the breakthrough curve to the models, it was determined that the model best able to adjust the data was the Thomas model, and the thermodynamic parameters of Cr(VI) and Ni(II) removal suggest that the process on YP is endothermic, while on OPB it is exothermic. In both biomaterials, the process is controlled by spontaneous chemisorption with a great affinity of the active centers for the ions.

Keywords: continuous system; metal ions; adsorption mechanisms



Citation: Villabona-Ortiz, A.; Tejada-Tovar, C.; González-Delgado, Á.D. Elimination of Chromium (VI) and Nickel (II) Ions in a Packed Column Using Oil Palm Bagasse and Yam Peels. *Water* **2022**, *14*, 1240. <https://doi.org/10.3390/w14081240>

Academic Editors: Cristina Palet and Julio Bastos-Arrieta

Received: 7 January 2022

Accepted: 8 April 2022

Published: 12 April 2022

Publisher's Note: MDPI stays neutral with regard to jurisdictional claims in published maps and institutional affiliations.



Copyright: © 2022 by the authors. Licensee MDPI, Basel, Switzerland. This article is an open access article distributed under the terms and conditions of the Creative Commons Attribution (CC BY) license (<https://creativecommons.org/licenses/by/4.0/>).

1. Introduction

The release of industrial sewage polluted with toxic heavy metals is a global environmental problem, because metals like chromium, mercury, cobalt, nickel, lead, copper, and arsenic [1] can have serious impacts on human, animal, and aquatic life, as they have a very stable nature and a reduced tendency toward the biodegradation of their compounds [2]. Among them, chromium and nickel are especially important, due to their multiple applications at the industrial level. Chrome compounds exist in water and soil, because of the industrial activities of tanneries, electronic manufacturing, pigments, fertilizers, textiles, and photography. Furthermore, when chromium comes into contact with water, it is toxic for living beings, because it is subjected to oxidation (III) and (VI) [3]. For this reason, Cr(VI) is considered a hazardous pollutant; normally, it occurs in chromate (CrO₄²⁻) or dichromate (Cr₂O₇²⁻) forms, and effortlessly trespasses biological barriers, while also being carcinogenic [4]. On the other hand, nickel is applied in manufacturing activities such as metallization, and in paint, electroplating, powder, batteries, and alloys, among other things, as well as in everyday products such as cosmetics, clothing, and electronic devices [5]. Ni(II) is toxic, and in high concentrations can cause lung, skin, cardiovascular, and gastrointestinal diseases, and even cancer [6].

Several methods have been implemented in the elimination of heavy metals from effluent, including precipitation, electro-flocculation, ionic exchange, solvent extraction, and osmosis; these methods have several disadvantages, including toxic sludge production, the need for chemical additives, energy requirements, and the generation of secondary contaminants [7]. For this reason, bioadsorption is presented as a viable, efficient, and non-destructive method for removing heavy metals from waste to address environmental problems [8]. Although adsorption has been widely used in the removal of heavy metals from water systems, this implementation has most commonly been used in batch systems. Among these, metal–organic frameworks have been used [9]. Additionally, nanomaterials and nanotechnologies have been developed that can be used to generate innovative materials that are able to provide water treatment plants with extraordinary properties, increasing cost efficiency [10].

Most of the research on Cr(VI) and Ni(II) bioadsorption has been performed using batch processes, because they are easy to apply on a small laboratory scale, but challenging to use on a massive scale, especially when the volume of industrial effluent is huge [11]. In addition, data from batch systems may not apply to continuous fixed-bed column operating conditions, where residence time is not necessary for achieving equilibrium [12]. Therefore, it is necessary to determine the real applicability of biosorbents in the continuous mode [13]. However, fixed-bed columns are preferred because of their high efficiency, easy method of operation, and ability to be expanded beyond laboratory scale to produce higher quality effluent [14]. Nevertheless, the use of eucalyptus in the elimination of Cr(VI) and Ni(II) in the packed-bed system has been reported [15], as well as palm residues [16], plantain waste [17], vetch [18], alharma [19] and kenaf [20], where the effects of temperature, pH, bed height and particle size were determined, presenting high percentages of removal.

Thus, in the present work, the performance of yam peel (YP) and oil palm bagasse (OPB) in the elimination of Cr(VI) and Ni(II) present in solution in a continuous system was evaluated, and the effects of temperature variation, particle size, and bed height were determined. The bioadsorbents were characterized using the proximal chemical analysis, FTIR (Fourier transform–infrared spectroscopy), SEM (scanning electron microscopy) and EDS (energy-dispersive X-ray spectroscopy) techniques.

2. Materials and Methods

2.1. Preparation of the Biomass

Oil palm bagasse (OPB) was obtained in Bolivar, Colombia, as a rejected by-product of the palm oil extraction process. Yam peel (YP) was obtained as post-harvest residues. Biomasses were selected in their best condition, washed with deionized water, sun-dried until a constant mass, and reduced in size in a blade mill; size classification was performed in a shaker-type sieve with stainless steel screens, selecting the particle diameters according to the design of the experiments.

2.2. Characterization of the Bioadsorbent

Proximal chemical analysis was performed using analytical methods to determine the content of pectin (thermogravimetry), lignin (acid digestion), cellulose (photolysis), hemicellulose (thermogravimetry digestion), carbon (AOAC 949.14), hydrogen (AOAC 949.14), nitrogen (AOAC 949.14-Kjeldahl), sulfur (948.13) and ash (nephelometry digestion). The functional groups and structural change in the biomass were determined by FTIR analysis of the bioadsorbents before and after adsorption using a Shimadzu IRAinfinity-1S spectrophotometer with a frequency of 32 scans between 600 and 4000 cm^{-1} . The surface properties of the biomasses were studied by SEM-EDS analysis using a scanning electron microscope coupled to an energy dispersive spectrophotometer model JSM-6490LV JEOL Ltd. (Tokyo, Japan).

2.3. Column Adsorption Tests

Adsorption tests were performed in packed-bed system following an experimental design created in Statgraphics Centurion XVI[®], with the central type composed of a 2³-rotating star on the response surface; there were 5 levels of temperature variation (30, 40, 55, 70 and 80 °C), particle size (0.1, 0.355, 0.5, 1 and 1.2 mm) and bed height (6.1, 30, 65, 100 and 124 mm), for a total of 16 experiments for each biomass–metal system. The experiments were conducted in an acrylic cylinder with height of 15 cm and internal diameter of 4.1 cm. The solution at 100 mg L⁻¹ was feed from a tank located at the top of the equipment, flowing into the column by gravity at a flowrate of 0.75 mL/s. To prepare the synthetic solutions, nickel sulfate (NiSO₄) and Potassium Dichromate (K₂Cr₂O₇) were used (Merck Millipore; Burlington, MA, USA) and dissolved in deionized water using pH of 2 and 6 for Cr(VI) and Ni(II), respectively.

The biomass packaging was filled with the biomaterials under study, and the conditions of temperature, bed height, and particle size were configured according to the proposed design of experiments. The samples were taken 5 min after starting the assays; the final concentration of Cr(VI) was determined by UV-Vis spectrophotometry at 540 nm in a Biobase spectrophotometer using phenolphthalein as an indicator, in accordance with ASTM D1687-17 [3]. The residual nickel (II) was determined using an atomic absorption spectrophotometer, Buck Scientific model 210 VGP, at 228.8 nm [5]. Adsorption efficiency was determined using Equation (1):

$$\%E = \frac{C_0 - C_i}{C_0} \times 100 \quad (1)$$

where C_0 is the initial concentration of the studied metal and C_i is the concentration of the studied metal after the adsorption process [21].

The effects of temperature, particle size, and bed height were studied using the Statgraphics Centurion software through the estimated response surface and the optimization of such response using the Surface Response Method (SRM), which made it possible to maximize the efficiency of the removal, determining the best conditions under which to construct the breakage curve.

2.4. Breakthrough Curve

The breakage curve or determining the time of service of the bed and the saturation of the biomaterial was constructed by means of continuous experiments under the optimum conditions obtained. The breakage curves for Cr(VI) and Ni(II) adsorption were adjusted to the models described below in OriginPro[®].

2.4.1. Thomas Model

This model obeys Langmuir's adsorption and considers the axial dispersion to be insignificant in the bed, because the driving force follows second-order kinetics with a reversible reaction given by Equation (2).

$$\frac{C_0}{C} = \frac{1}{1 + \exp\left[\frac{K_{th}}{Q} (q_0 X - C_0 V)\right]} \quad (2)$$

where K_{th} is Thomas' constant (mL min⁻¹ mg⁻¹); q_0 is the maximum concentration of solute in the solid phase (mg g⁻¹); X is the amount of adsorbent in column (g), Q is the rate of flow (mL min⁻¹), and V (L) is the volume of the effluent at the time of operation.

2.4.2. Yoon–Nelson Model

Yoon–Nelson model. This model relates the dimensionless parameter C/C_0 throughout the operating time by means of two parameters, K_{YN} and τ , which correspond to the

proportionality constant in min^{-1} and the time after which 50% of the initial adsorbate is retained, respectively. This is shown in Equation (3).

$$\frac{C}{C_0} = \frac{\exp(K_{YN}t - \tau K_{YN})}{1 + \exp(K_{YN}t - \tau K_{YN})} \quad (3)$$

2.4.3. Dose–Response (DR) Model

The DR model can be represented by Equation (4).

$$\frac{C}{C_0} = 1 - \frac{1}{1 + \left[\frac{C_0 \times Q t}{q_0 X} \right]^a} \quad (4)$$

where a is the constant of the model; q_0 is the maximum solute concentration in the solid phase (mg g^{-1}), X is the amount of adsorbent in the column (g), and Q is the rate of flow (mL min^{-1}).

2.4.4. Adams–Bohart Model

This model is implemented to describe the initial part of the breakage curve above the breakage or saturation points, assuming that the adsorption velocity is proportional to the adsorption capacity and the concentration of the adsorbed species. This model is described according to Equation (5).

$$\frac{C}{C_0} = \frac{\exp(K_{AB}C_0t)}{\exp\left(\frac{K_{AB}N_0L}{v}\right) - 1 + \exp(K_{AB}C_0t)} \quad (5)$$

where K_{AB} is the kinetic constant of Adams–Bohart in ($\text{L/mg}\cdot\text{min}$), N_0 is the maximum volumetric adsorption capacity in mg L^{-1} , v is the linear flow rate in (cm/min), L is the depth of the column bed in cm, C_0 is the internal concentration mg L^{-1} , C_t is the concentration of the effluent, and t is the residence time of the dissolution in the column.

2.4.5. Adsorption Capacity of the Column

The adsorption capacity of the column was determined using Equation (6).

$$q_j = \frac{C_j^f Q}{1000m_s} \int_0^{t_s} \left(1 - \frac{C_j^{out}}{C_j^f} \right) dt \quad (6)$$

where q_j is the concentration of the ion in the adsorbent (mmol/gram), C_{jf} is the feed concentration of the j -ion in the liquid phase (mmol/L), Q is the volumetric flow rate of the solution flowing through the column (cm^3/min), m_s is the mass of the biomass with which the tower is packed (g), C_j^{out} is the j -ion output concentration in the liquid phase (mmol/L), and t_s is the time at which the column is saturated (min) [22].

2.5. Thermodynamic Parameters

To establish in a general way the type of adsorption of the metals using OPB and YP, the equilibrium constant K_c and the values of adsorption enthalpy (ΔH°), adsorption entropy (ΔS°), and Gibbs' energy (ΔG°) were determined, making it possible to establish the favorability of the process and the effect that the temperature has on it [23]. For this, Van't Hoff's graphical method was used, according to the following equations:

$$\Delta G = \Delta H - T\Delta S \quad (7)$$

$$G = -RT \times \ln k_c \quad (8)$$

$$\ln K_c = \frac{-\Delta H}{RT} + \frac{\Delta S}{R} \quad (9)$$

3. Results

3.1. Characterization of Bioadsorbents

The bromatological analysis of OPB and YP is shown in Figure 1, where it can be seen that the compounds with the greatest presence in both biomaterials are lignin and cellulose, compounds which stand out for having hydroxyl, carboxyl, and phenolic functional groups in their structure, and which are important in the adsorption of metallic ions [24].

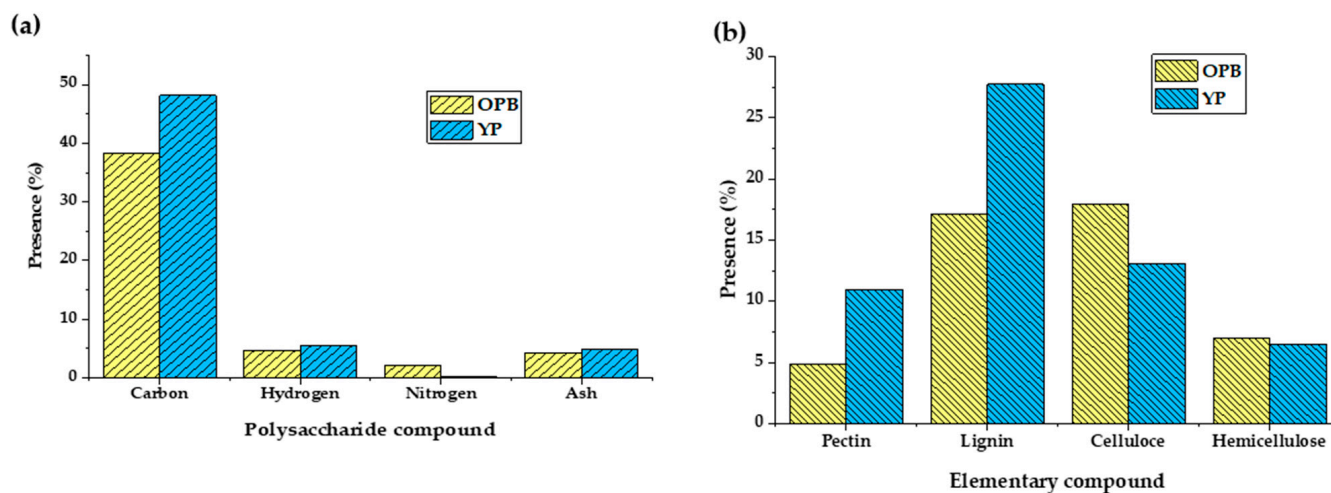


Figure 1. Bromatological analysis of OPB and YP: (a) polysaccharide compounds and (b) elementary compounds [25,26].

The most abundant element in the two bioadsorbents is carbon, which is typical of lignocellulosic materials due to the presence of lignin, cellulose, and hemicellulose. Therefore, a high efficiency of Cr(VI) and Ni(II) adsorption is expected, because these compounds are known to possess a large number of OH⁻ groups [27], carboxyl, and phenol, which can promote the adsorption of heavy metals [28]. Similarly, it can be observed that the lignin content in YP and OPB is high, and therefore the removal efficiency may be higher in these materials [29]. The ash content is higher than 4% in both biomaterials, indicating that the biomass contains in its structure oxides of silica, aluminum, iron, calcium, magnesium, titanium, sodium, and potassium [30].

The FTIR spectrum was obtained for OPB and YP before and after the Cr(VI) and Ni(II) adsorption processes (Figures 2 and 3). For both adsorbents, the evident stretching between frequencies of 3500 and 3800 cm⁻¹ corresponds to the hydroxyl (O-H) functional group [31], while the presence of primary and secondary amines is indicated by the stretching of the N-H bond between 3200 and 3450 cm⁻¹ [32]. Additionally, stretching and deformation of the C-H group and carboxylic acid can be observed between the frequencies of 2700 and 3000 cm⁻¹, as well as the stretching of carbon dioxide O=C=O close to the band at 2400 cm⁻¹ [33]. The vibrations between 900 and 1800 cm⁻¹ are attributed to alkenes, aromatics, and carboxylic acids [19]. Around the band between 1600 and 1650 cm⁻¹, a stretch of the carbonyl group of pectin, cellulose, and hemicellulose carboxylic acids can be observed, while between 900 and 1200 cm⁻¹, vibrations corresponding to the C-O group of alcohols and phenols are evident [28]. The presence of these multiple adsorption peaks confirms the heterogeneous nature and structural complexity of the bioadsorbents under study.

In the FTIR spectrum of the OPB and the YP following Cr(VI) and Ni(II) adsorption, changes in the functional groups of the biomasses can be observed, and the difference in the vibrations is remarkable. This is attributed to the incorporation of the metals under study onto the surface of the biomass, whereby they are joined to different functional groups on it [34]. The change in the intensity of the bands of the groups OH, CH, CO, NH, and C=C evidences the union of the ions; active and present functional groups in the biomass are key to the mechanism of adsorption of cationic pollutants [35]. Between 900 and 1800 cm⁻¹, the

presence of aromatic rings in the lignin and stretching of the C-O groups can be observed [4]. The vibrations of the bands between 700 and 1300 cm^{-1} present inorganic groups [36].

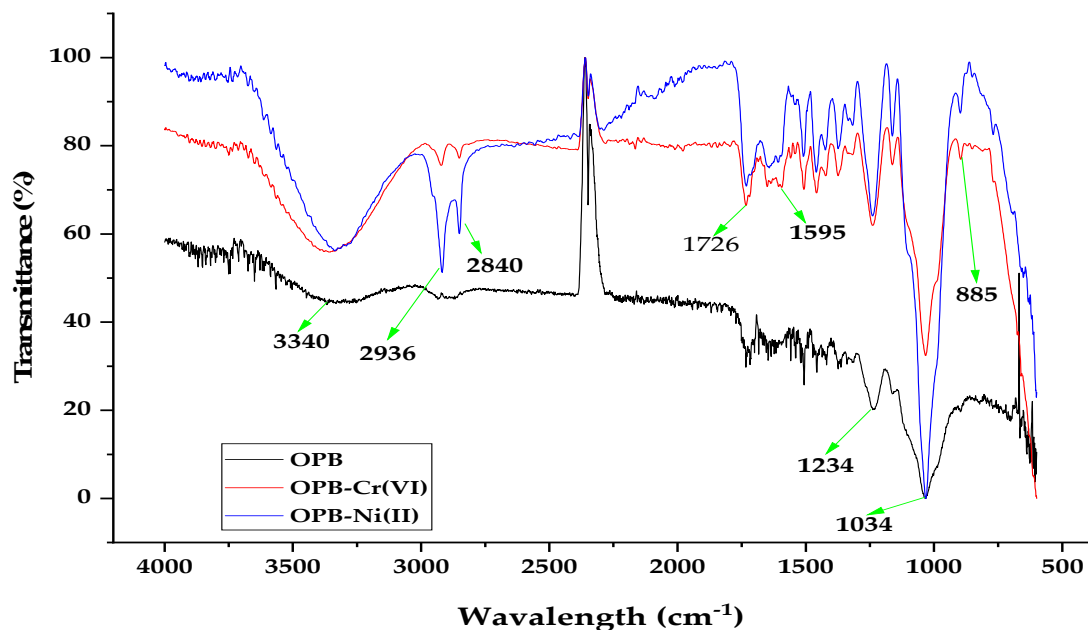


Figure 2. OPB FTIR before and after Cr(VI) and Ni(II) adsorption.

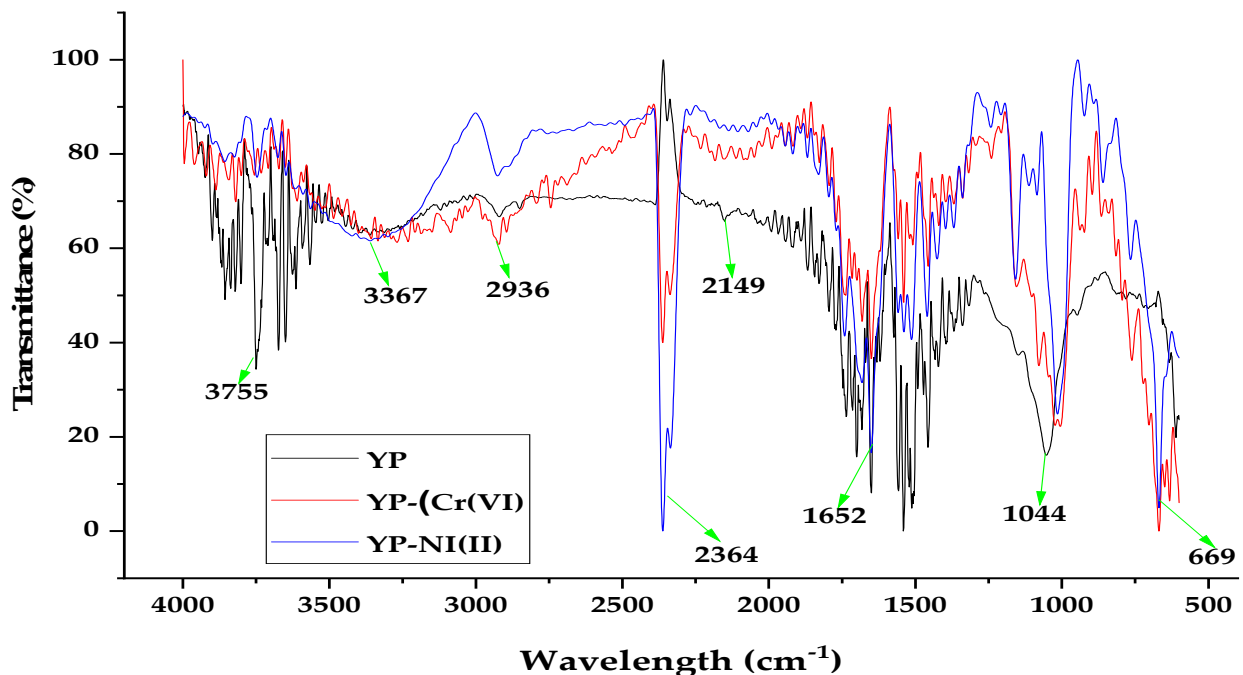


Figure 3. FTIR analysis of yam peels before and after removal of Cr(VI) and Ni(II).

In Figure 4 and Table 1, it can be seen that YP exhibits an irregular surface with the presence of mesopores, while the morphology of OPB is fibrous, with the presence of porosity and cavities [26]. Carbon, calcium, and oxygen are present in both materials, with YP exhibiting the most diverse structure, with traces of multiple elements such as potassium, silicon, aluminum, phosphorus, and iron, among others [37]. The presence of these elements is related to the functional groups present in lignocellulosic materials (cellulose, hemicellulose, lignin, and pectin) [4] and its ability to capture cations due to electrostatic forces; therefore, white particles are observed on the micrographs [38]. It is

evident that the pores of the biomaterials are covered by the metals following adsorption, and so they are softened when they are covered by Cr(VI) and Ni(II) [39].

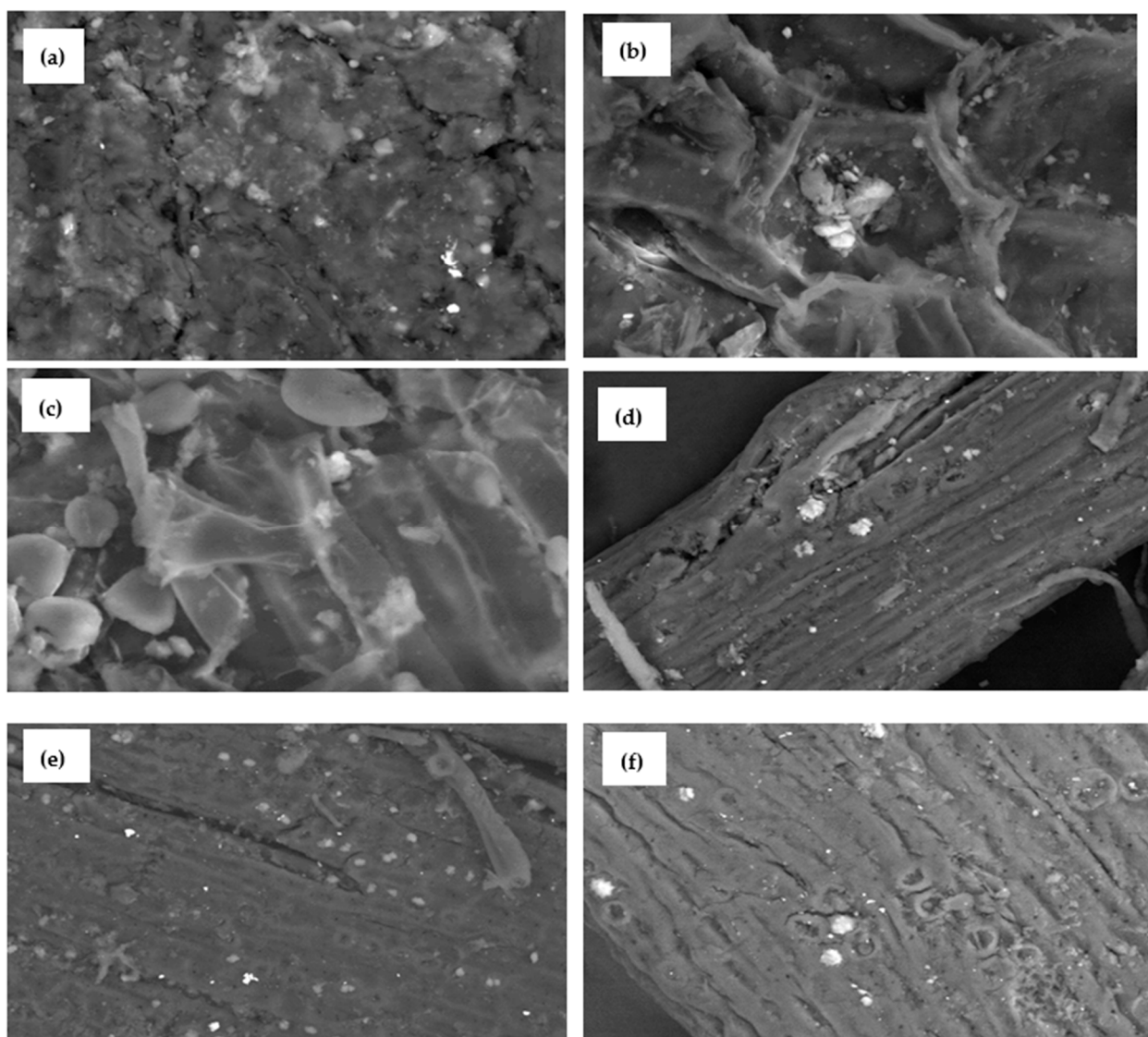


Figure 4. SEM micrograph of OPB (a) before the adsorption process, and (b) yam after the Cr(VI) adsorption process and (c) after the Ni(II) adsorption process; and YP (d) before the adsorption process, and (e) yam after the Cr(VI) adsorption process and (f) after the Ni(II) adsorption process; SEM micrographs have magnification $\times 500$.

With respect to SEM and EDS after adsorption, the presence of Cr(VI) was observed on the basis of the characteristic high-intensity peaks at 1, 5.6, and 5.8 keV, while the appearance of Ni(II) was found on the basis of the peaks at 1.4, 7.8 and 8.2 keV. Due to the structural changes reflected in the FTIR (Figures 1 and 2) and the EDS spectra after adsorption, as well as the increase in the number of white particles precipitated onto the surface of the two adsorbents, it can be established that the mechanism of adsorption of both metals in the biomaterials is an exchange between the studied cations and the dispoible centers of the material [40], which promotes the formation of microcomplexes and precipitation [41] when Cr(VI) and Ni(II) are retained at the active centers [42]. In the EDS after Cr(VI) adsorption, a decrease in Ca intensity of 0.2 keV was observed in OPB, while the intensity of O increased at 0.6 keV, and K appeared at 3.6 keV; meanwhile, YP presented a decrease in the peaks of Ca at 0.6 keV, Fe at 1.1 keV, and K at 3.6 keV, while P disappeared at 2.0 keV and S at 2.1 keV. Following the removal of Ni(II), OPB

presented an increase in the Fe peak at 0.8 keV, and the appearance of Al at 1.8 keV, S at 2.2 keV, Fe at 6.6, and 6.9 keV, while in YO presented the disappearance of P at 2.0 keV, Al at 1.8 keV, S at 2.1 keV, Fe at 0.7 keV, 6.5 keV, and 7.7 keV, and Cu at 0.9 keV, 8 keV, and 8.6 keV; there was also a decrease in the peaks for K at 3.4 keV and Ca at 0.2 keV and 3.8 keV; the disappearance of these compounds in the structure of the biomaterials was due to the formation of links with the heavy metals, and their entry into the lignocellulosic structure is shown in the FTIR spectra (Figures 2 and 3), corroborating that ion exchange is the mechanism of adsorption [28]. The above occurred along with slight variations in the intensity of the peaks marking the presence of Ca, while a new peak of Cr(VI) and Ni(II) was observed with the C, N, K, Na, Mg, Al, silicon, chlorine and Ca groups contained on the surface, confirming the adsorption of the heavy metals under study [39].

Table 1. EDS compositional analysis.

Element	OPB		OPB—Cr(VI)		YP		YP—Cr(VI)	
	Weight %	Atomic %	Weight %	Atomic %	Weight %	Atomic %	Weight %	Atomic %
C	50.90	59.07	48.65	56.49	47.40	57.07	54.50	63.25
O	44.60	38.85	48.82	42.56	43.20	39.05	39.67	34.56
Al					0.75	0.40	0.82	0.42
Si	3.87	1.92	1.12	0.56	2.16	1.11	1.21	0.60
P					0.66	0.31		
S					0.17	0.08		
K			0.20	0.07	4.46	1.65	0.44	0.16
Ca	0.19	0.07	0.25	0.09	0.34	0.12	0.99	0.34
Fe					0.60	0.16	0.59	0.15
Cu	0.45	0.10	0.49	0.11	0.27	0.06	0.45	0.10
Cl							0.45	0.18
Cr			0.48	0.13			0.88	0.24
Totals	100.00	100.00	100.00	100.00	100.00	100.00	100.00	100.00

3.2. Adsorption Tests

Tables 2 and 3 summarize the results of Cr(VI) and Ni(II) adsorption on OPB and YP under the evaluated conditions. For the removal of Cr(VI) and Ni(II) using OPB, the results were very similar under all of the evaluated operating conditions; therefore, a deeper statistical analysis was necessary in order to be able to draw any conclusions (see Section 3.3). This can be explained by the fact that OPB, as a fibrous material, ensures the tortuosity of the bed, regardless of the bed height.

On the other hand, when using YP, the best conditions, found on the basis of optimization analysis, for Cr(VI) removal were a particle size of 0.355, a temperature of 55 °C and a bed height of 89 mm, while for Ni(II), they were a particle size of 1 mm, a temperature of 70 °C, and a bed height of 123 mm (Table 3).

OPB exhibits a high efficiency of Ni(II) and Cr(VI) removal, with percentages higher than 87%; this is due to the heterogeneity of the biomass due to its lignocellulosic character, which ensures the presence of hydroxyl, carboxyl, amino, unsaturated hydrocarbon, and phenol groups, which have a direct influence on the removal of these ions [43]. Despite the good performance of the bioadsorbent for the two metals, there is evidence of better behavior with respect to Cr(IV), which can be explained by their ionic radius: Cr(VI) has an ionic radius of 0.69, while Ni(II) has an ionic radius of 0.78, and the lower ionic radius increases the diffusion of the metal in solution and on potential adsorption sites [44]. Regarding the evaluated variables, an increase in temperature from 30 °C to 55 °C decreases the retention of both metals on OPB and YP, while at temperatures greater than 55 °C, increasing temperature results in a slight increase in removal efficiency. This may be due to the fact that the increase in temperature contributes to an increase in the speed of the ions within the solution and the biomass, counterbalancing the thermodynamic effect, which in turn causes a reversal of the trend whereby the temperature continues to increase [45].

Considering the high degree of removal achieved by the biomass, the effect of this variable is considered to be insignificant, since it does not constitute a determining aspect for the process, suggesting that energy changes in the system do not have an important effect on the mass transfer mechanisms that allow the diffusion of ions on the biomass. However, variation in temperature is important, since it constitutes a critical variable when scaling the process up. Therefore, it is considered that the best conditions for carrying out the removal exist at room temperature. The influence of bed height presents a positive behavior when using the two adsorbents, removal efficiency increasing with increasing bed height, which can be explained by the availability of a greater number of link sites for adsorption and the increased residence time. Therefore, the diffusion of the ions is more effective, since the contact between the phases is more intimate [17].

Table 2. Cr(VI) and Ni(II) removal efficiency over OPB in a continuous system.

Temperature (°C)	Particle Size (mm)	Bed Height (mm)	OPB	
			Cr(VI)	Ni(II)
70	0.355	30.0	100.00	99.86
40	0.355	100.0	99.97	99.53
55	0.500	6.13	99.98	89.85
70	1.000	30.0	99.99	87.24
40	1.000	30.0	100.00	90.37
40	0.355	30.0	100.00	98.93
70	0.355	100.0	99.98	99.57
30	0.500	65.0	100.00	98.33
40	1.000	100.0	99.97	97.16
70	1.000	100.0	99.99	96.77
55	0.500	123.9	99.99	99.76
55	0.500	65.0	99.99	96.80
80	0.500	65.0	100.00	96.95
55	0.500	65.0	99.99	96.80
55	0.135	65.0	99.98	99.76
55	1.219	65.0	99.99	91.18
55	0.500	65.0	99.99	96.80

Table 3. Cr(VI) and Ni(II) removal efficiency over YP in a continuous system.

Temperature (°C)	Particle Size (mm)	Bed Height (mm)	YP	
			Cr(VI)	Ni(II)
70	0.355	30.0	96.26	96.65
40	0.355	100.0	87.30	87.4
55	0.500	6.13	65.30	91.40
70	1.000	30.0	97.43	90.20
40	1.000	30.0	98.30	96.72
40	0.355	30.0	96.95	95.22
70	0.355	100.0	87.01	87.0
30	0.500	65.0	87.70	94.46
40	1.000	100.0	88.24	94.07
70	1.000	100.0	91.10	95.91
55	0.500	123.9	92.30	98.74
55	0.500	65.0	94.50	98.17
80	0.500	65.0	94.88	98.82
55	0.500	65.0	97.32	97.25
55	0.135	65.0	87.1	87.2
55	1.219	65.0	98.01	91.66
55	0.500	65.0	94.50	98.15

On the other hand, the increase in particle size positively affects the influence of Cr(VI) removal when OPB is used, which is decisive for establishing the hydrodynamics of the

adsorption column, and thus the prevention of overflow [46]. Meanwhile, removing Ni(II) using OPB as well as using YP to remove both metals is favored by decreased particle diameter due to increased area of contact exposed to the smaller particle size; this, in turn, favors the diffusion velocity [47]. However, in practice, for packed-bed systems in which the flow is continuous, very small particle sizes are inadequate, because the close spacing between the bed particles leaves less space for the transit of the fluid, affecting the tortuosity of the bed. In fact, while executing the experiment, it was noticed that the smaller particle sizes caused an obstruction of the fluid on the bed, making its transit difficult; this represents a difficulty, since the ideal is to treat as much of the solution as possible without decreasing the quality of the removal achieved during operation. In this case, sacrificing a small amount of the optimal particle size can lead to better operation of the system, without sacrificing much of the effectiveness of the operation.

Table 4 shows the q_{max} data of the parameters reported for the removal of Cr(VI) and Ni(II) with different evaluated adsorbents, showing that the results obtained in the present study lie in the average range for bioadsorbents of lignocellulosic origin.

Table 4. q_{max} of Cr(VI) and Ni(II) in a fixed bed using various adsorbents.

Metal	Adsorbent	Conditions	q_{max} (mg/g)	Reference
Cr(VI)	Pecan nut husk	0.85 mm particle size, pH = 6.2	180.75	[4]
	Eucalyptus	pH = 2, 15 cm bed height, 50 mg/L initial concentration	381.82	[15]
	Palm Oil Fuel Ash	100 mg/L initial concentration, 36.4 g adsorbent, pH = 2.	0.41	[16]
	Biosynthesized melanin-coated PVDF membranes	0.5 mL/min, 3 mg/L, 10 mg adsorbent	9.29	[28]
	Plantain starch residues	0.75 mL/s, 100 mg/L initial concentration, pH = 2, 68 °C, 81.49 mm bed height	29.85	[17]
Ni (II)	OPB	0.75 mL/s, 100 mg/L initial concentration, pH = 2	115.45	This work
	YP		50.12	
	Plantain starch residues	0.75 mL/s, 100 mg/L initial concentration, pH = 6	28.01	[22]
	Yam starch residues		22.08	
	Fenton modified with <i>Hydrilla verticillate</i>	Bed height = 25 cm, 10 mL/min, initial concentration 5 mg/L	87.18	[48]
	Carboxylated sugarcane bagasse	25 °C, pH = 5.5, 0.5 g adsorbent	1020	[49]
	OPB	0.75 mL/s, 100 mg/L initial concentration, pH = 6, 55 °C	103.49	This work
YP	30.04			

3.3. Application of the Surface Response Method (SRM)

SRM was applied to the experimental data using the Statgraphics Centurion software, and a mathematical expression of adsorption efficiency was obtained that fits the results of the experimental results presented in Tables 2 and 3; in this way, it was possible to vary the parameters of the factors temperature, particle size, and bed height by means of Equation (10) for Cr(VI) and Equation (11) for Ni(II), using OPB as the adsorbent.

$$\begin{aligned} \%R = & 100.04838 - 0.0014138539 A - 0.046518846 B \\ & - 0.00033061127 C + 0.0000076169902 A^2 \\ & - 0.00010335917 A B + 0.0000071428571 A C \\ & + 0.041973067 B^2 + 0.000022148394 B C + 3.8888414E \\ & - 7 A^2 \end{aligned} \quad (10)$$

$$\begin{aligned} \%R = & 105.71338 - 0.14294739 A - 9.4454119 B - 0.007324277 C \\ & + 0.00153546 A^2 - 0.11583979 A B \\ & + 0.00044214286 A C - 3.7284854 B^2 + 0.17744186 B C \\ & - 0.00052249029 C^2 \end{aligned} \quad (11)$$

where %R is the percentage removal, A is the temperature in °C, B is the particle size in mm, and C is the bed height in mm. Using these equations, graphs of the estimated response surface were obtained (Figure 5), which described the influence of the evaluated variables on the processes of Cr(VI) and Ni(II) adsorption on OPB. The concave downwards shape indicates the adverse effect of increasing temperature and particle size at different bed heights. The optimal conditions for maximizing the removal efficiency of the process were obtained as follows: temperature of 40 °C, particle size of 1 mm size, and bed height of 30 cm for Cr(VI), while for Ni(II) these values were a temperature of 80 °C, particle size of 0.212 mm, and a bed height of 50.3 mm. The breakage curve of the two metals on OPB was constructed under these optimal conditions.

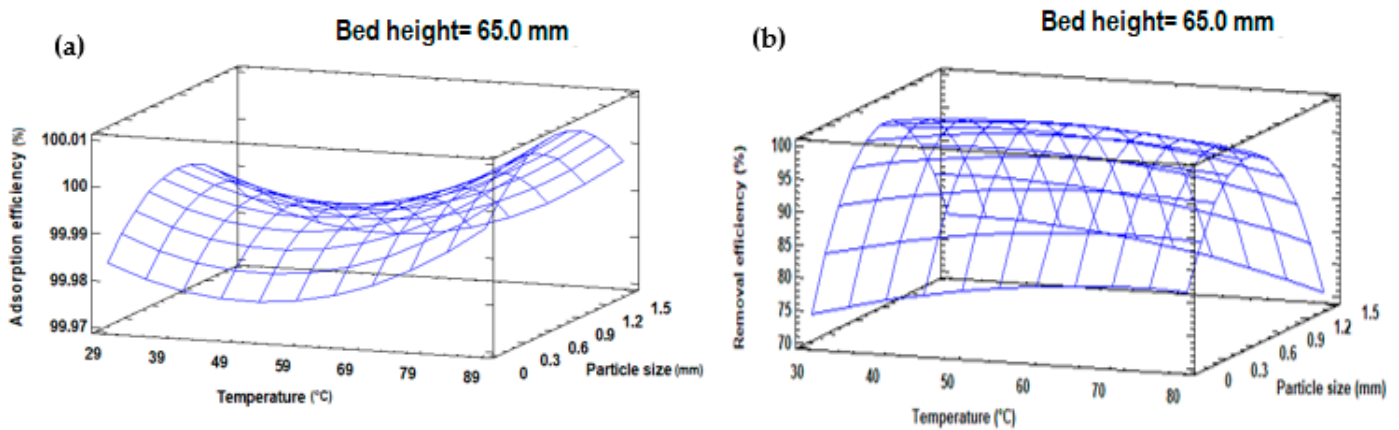


Figure 5. Estimated response area for the removal efficiency of (a) Cr(VI) and (b) Ni(II) on OPB.

Previous studies on Cr(VI) and Ni(II) adsorption on Fenton *Hydrilla verticillata* (FMB)-modified dry biomass in industrial waste, in which the effect of bed height, flow rate, influent metal ion concentration, and particle size were evaluated, concluded that the values most favorable for the removal of heavy metals were the highest bed height (25 cm); a lower flow rate (10 mL min⁻¹), and a lower concentration of influential metal (5 mg L⁻¹), in order to ensure optimal tortuosity and hydrodynamic conditions with the aim of maximizing bed removal [48].

Regarding the application of SRM to the results obtained for the adsorption of Cr(VI) and Ni(II) on YP, Equations (12) and (13) were obtained for the two metals, respectively, where %R is the percentage of removal, A is the temperature in °C, B is particle size in mm, and C is the bed height in mm.

$$\%R = 77.51 - 0.0065A - 2.622B B + 0.45C - 0.0018 A^2 + 0.18 A B + 0.0019 A C + 0.426 B^2 - 0.0165 B C - 0.0039C^2 \tag{12}$$

$$\%R = 77.67 + 0.438A + 17.45B - 0.0228C - 0.0035A^2 + 0.11AB - 0.000826AC - 32.23B^2 + 0.338BC - 0.0011B^2 \tag{13}$$

From these equations, the estimated response surface was obtained (Figure 6), and the significant positive effect of increasing particle size on the quantity of Cr(VI) elimination was observed, while the concave shape of the scheme for nickel shows that intermediate values of the considered variables favored its removal. In addition, a temperature of 62 °C, a particle size of 1.22, and a bed height of 89.3 mm were determined to be the optimal conditions for the removal of Cr(VI), while for Ni(II) these parameters were a temperature of 70 °C, a particle size of 1 mm, and a bed height of 123.8 mm. The breakage curve was constructed under these conditions.

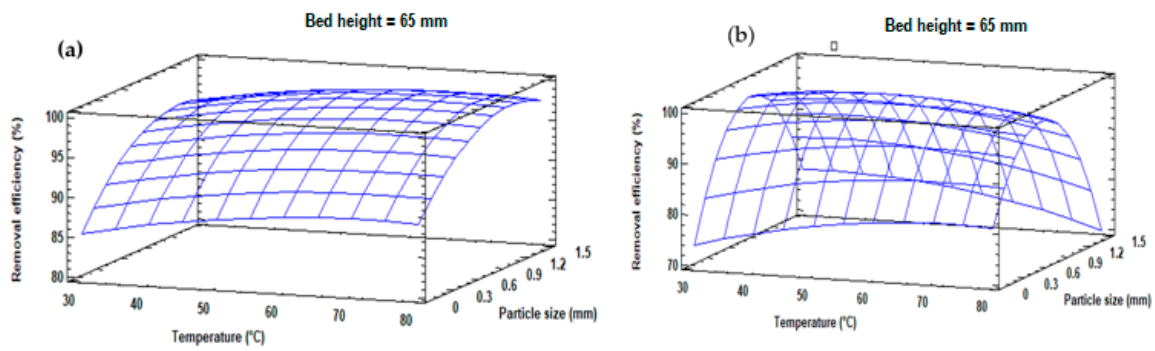


Figure 6. Estimated response area for the removal efficiency of (a) Cr(VI) and (b) Ni(II) on YP.

The optimization of the response variable was obtained using the RSM methodology, as shown in Table 5. The experiments for analyzing the breakage curve were performed under these conditions.

Table 5. Optimization of removal efficiency of Cr(VI) and Ni(II) over OPB and YP.

Factor	OPB		YP	
	Cr(VI)	Ni(II)	Cr(VI)	Ni(II)
Temperature (°C)	30	80	55	70
Particle size (mm)	0.5	0.212	0.355	1
Bed height (mm)	65	50.3	89	123

3.4. Breakthrough Curve

The breakage curve shows the performance of a fixed-bed column in terms of the amount of metal that can be retained, expressed in terms of a standardized concentration (C/C_i), as a function of time or effluent volume for a fixed bed height [50]. For this study, the breakpoint was established as the point at which the concentration at the end of the column reached 0.1% of the C_i , while the concentration at which 95% was reached was established as the column saturation point [20]. Figure 7 shows the Cr(VI) and Ni(II) breakage curves on OPB and YP, which were made at the best conditions found and at 100 mg L^{-1} .

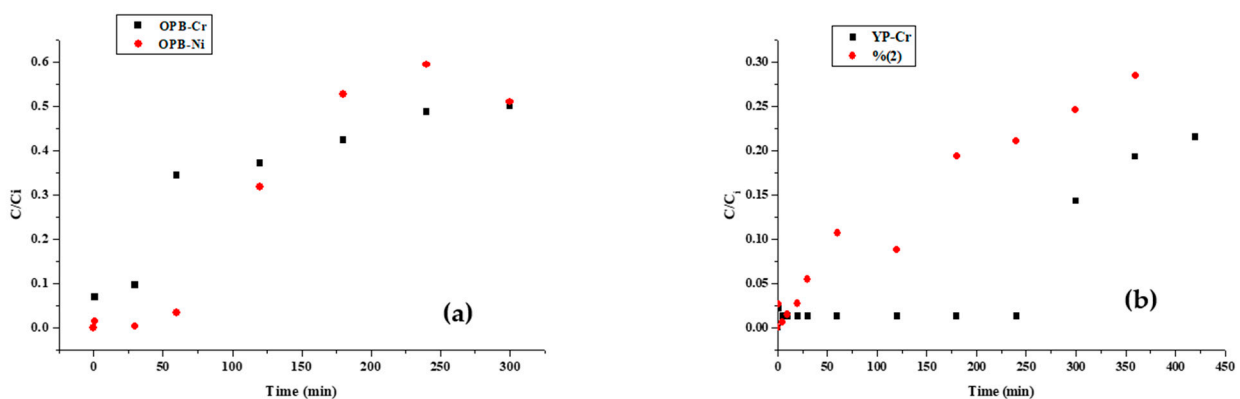


Figure 7. Breakage curve for the adsorption of Cr(VI) and Ni(II) on (a) OPB and (b) YP.

The experimental data obtained from experiments were analyzed to evaluate the effect on the C_f/C_i vs. time plot, and to establish the q (mg/g) of the bed. It was evidenced that the highest adsorption of metal ions occurred at the beginning of the tests, due to the high disposal of active sites in the unsaturated bioadsorbent [31].

As a result, metal ions were retained around or inside the active sites, while the effluent from the end of the bed was almost raw without the presence of the cations. As the bed operation time passed, its capability to capture ions progressively diminished due to the

occupation of the existing active sites; therefore, the concentration of the effluent increased until the outlet concentration was 30% of the inlet concentration [21]. However, the total saturation of the adsorbent was not reached in the column, so the breakage curve exhibits an upward trend after the contact time. Applying Equation (3), the maximum adsorption capacity of the column was determined for each adsorbent–metal system, indicating that the highest adsorption capacities were obtained for Cr(VI), with 111.45 mg g⁻¹ and 50.12 mg g⁻¹ on OPB and YP, respectively; meanwhile, for Ni(II), values of 103.49 mg g⁻¹ and 30.04 mg g⁻¹ were obtained. With respect to the values obtained for the removal of Ni(II) on OPB (*Elaeis guineensis*) in stages, a q_e of 103.3 mg g⁻¹ biomass was reported for bagasse, which is very close to the value obtained in the present study [51], which is superior to those reported by [22] using plantain, yam and OPB residues, respectively. Likewise, the results of Cr(VI) removal using OPB and YP are superior to those obtained in other studies, where 29.85 mg g⁻¹ on plantain residues was achieved [17]. The experimental adsorption capacity for the removal process of both metals in the column was higher for palm bagasse; this is attributed to its highly porous nature and the typical fibrous surface of lignocellulosic materials [52].

On the other hand, designing a continuous adsorption system requires knowing mainly its adsorption profile (concentration–time), so there are different theoretical models that seek to describe the behavior of a column, estimating some kinetic parameters [21]. Breakage curve data were fitted to the Dose–Response, Yoon–Nelson, Adams–Bohart, and Thomas models. The fitting parameters are summarized in Table 6.

Table 6. Adjustment parameters for Cr(VI) and Ni(II) adsorption on OPB and YP using non-linear regression.

Model	Parameter	OPB-Cr	OPB-Ni	YP-Cr	YP-Ni
Thomas	K_{Th} (mL min ⁻¹ mg ⁻¹)	0.06	0.077	0.09	0.06
	q_{Th} (mg g ⁻¹)	58.85	27.69	47.58	23.94
	R ²	0.66	0.55	0.87	0.84
Dose-Response	q_{D-R} (mg g ⁻¹)	62.18	24.74	54.21	54.93
	a	0.67	1.29	2.85	0.84
	R ²	0.91	0.86	0.92	0.95
Yoon–Nelson	K_{Y-N} (min ⁻¹)	0.00616	0.01	0.008615	0.00609
	τ (min)	255.9752	269.36	533.67	486.79
	R ²	0.66	0.55	0.87	0.8391
Adams–Bohart	K_{A-B} (L min ⁻¹ mg ⁻¹)	3.622×10^{-5}	4.09×10^{-5}	7.43×10^{-5}	4.98×10^{-5}
	N_0 (mg L ⁻¹)	39388.88	15013.42	13281.04	9302.27
	R ²	0.53	0.21	0.85	0.81

From the data presented in Table 6, it can be stated that, according to their respective square correlation coefficients, the experimental Cr(VI) and Ni(II) removal data on YP and OPB best fit the DR model, with R² exceeding 90%. Considering the industrial implementations of adsorption, the established advance time defines the operational limits of the column; however, in the present study, such saturation was not reached. Rather, it was established that all the biomasses could be used during the study time, since they present a high heavy metal adsorption capacity, as reported when Fenton-modified *Hydrilla verticillata* biomass was used as Cr(VI) and Ni(II) adsorbents [48]. Despite the R² value reported for the DR model, it was observed that the q reported by this model when using OPB to remove the two metals was much lower than that obtained experimentally. Similarly, the theoretical q obtained by the models was much higher than the experimental q with YP; in this sense, the model that comes closest to the experimental values is the Thomas model, so it was assumed that the mechanism of adsorption was Langmuir-type adsorption followed by chemical sorption of a pseudo-second-order monolayer, which is evident in the precipitation and micro complex formation evidenced in the SEM micrographs reported in Figures 3 and 4 [36]. The prediction of the breakage curve by the Thomas model has

previously been reported by Srivastava et al. [36], Nordin et al. [16], and Xavier [49] using red beans impregnated with nanoparticles of magnetite, OPB and carboxylated OPB resin. It has been reported, when using mangosteen peel for Cd(II), that the good fit of the data using the Thomas model suggests that external and internal diffusion will not be the limiting step [6].

3.5. Thermodynamic Parameters

It is established on the basis of the positive sign of ΔH° that the processes of removal of Cr(VI) on OPB and YP is of an endothermic nature, such that the energy must be proportional to the system in order to boost diffusive phenomena (Table 7) [22]. It also follows that the limiting step of chromium adsorption on OPB and YP is the chemical adsorption [53]. In addition, the positive values of ΔG° for Cr(VI) removal onto the two evaluated adsorbents suggest that the system is non-spontaneous, and the increase in the module with increasing temperature indicates that the process becomes energetically more favorable [54]. The positive value of ΔS° exposes the high affinity of Cr(VI) ions with biomaterials and also the possibility of some structural modifications due to the development of links with functional groups at the interface, as well as high randomness at the solid–solution interface, as shown by FTIR spectra and SEM-EDS analysis; it is also inferred that the process is reversible.

Table 7. Thermodynamic parameters for chromium (VI) and nickel (II) adsorption at bed height of 65 mm.

Biomass	Cr (VI)					Ni (II)			
	T (K)	q_e (mg/g)	ΔG° (kJ/mol)	ΔH° (kJ/mol)	ΔS° (kJ/mol \times K)	ΔG° (kJ/mol)	ΔH° (kJ/mol)	ΔS° (kJ/mol \times K)	
OPB	303.15	0.79	30.19	3.46	28.81	0.79	−84.29	−107.32	−25.91
	328.15	0.78	32.68			0.78	−91.25		
	353.15	0.78	35.17			0.78	−98.20		
YP	303.15	2.70	20.16	18.65	6.59	−75.54	−19.65	−24.98	
	328.15	2.91	21.80			−81.79			
	353.15	2.92	23.45			−88.03			

For Ni(II), the ΔH° values establish that the removal process possesses an exothermic nature and occurs by physisorption [53]. ΔG° values indicate the spontaneity of the process and that it becomes energetically more favorable, evolving by itself. On the basis of the negative magnitude of ΔS° , it can be said that the bond between the metal and the biomass is strong, with a low possibility of desorption [54].

The difference found in the adsorption mechanism regarding the thermodynamic parameters may be in accordance with the chemical nature of Cr(VI) and Ni(II), and its influence over the chemical interactions with the active centers in the adsorbent; thus, the different valences, atomic ratios and the ionic energies between the heavy metals cause the energetic requirements for each case to be specific. When using eucalyptus as an adsorbent of Cr(VI), equal results were obtained [15], as well as when using nanocellulose modified with polypyrrole [55], in addition to when using pea peels [18] and composites of Polyaniline and Iron Oxide [56] for removing Ni(II) ions.

4. Conclusions

The monocomponent elimination of Cr(VI) and Ni(II) on OPB and YP was performed. The morphological and physical characterizations showed a porous, heterogeneous structure with high presence of functional groups that favor heavy metal adsorption processes. The SEM-EDS results suggest that the adsorption mechanism that controls the process is cation exchange with the active sites of the adsorbent, as well as precipitation and complexing on the exposed surface of the biomaterials. From the adsorption essays, removal efficiencies above 80% were obtained in all cases, presenting better performance in Cr(VI) removal due to its diffusion capacity through the bioadsorbent pores. Statistical analysis shows that particle size was the most significant factor in the adsorption processes.

Maximum capacities of Cr(VI) of 111.45 mg g⁻¹ and 50.12 mg g⁻¹ were achieved on OPB and YP, respectively; while for nickel, capacities of 103.49 mg g⁻¹ and 30.04 mg g⁻¹ were obtained. The Thomas model fitted very well to the experimental breakage curves, so it is assumed that monolayer adsorption was followed by chemisorption. Thermodynamic study suggested an endothermic process that was non-spontaneous, with high affinity between Cr(VI) and the adsorbents; meanwhile, Ni(II) adsorption onto OPB and YP exhibited an exothermic and spontaneous nature.

Author Contributions: Conceptualization, C.T.-T., A.V.-O. and Á.D.G.-D.; methodology, C.T.-T.; software, A.V.-O.; validation, C.T.-T., A.V.-O. and Á.D.G.-D.; formal analysis; investigation; resources, C.T.-T.; data curation, Á.D.G.-D. writing—original draft preparation; writing—review and editing, C.T.-T.; visualization, A.V.-O.; supervision, C.T.-T.; project administration, A.V.-O. and Á.D.G.-D.; funding acquisition, C.T.-T. All authors have read and agreed to the published version of the manuscript.

Funding: This research received no external funding.

Data Availability Statement: The data that support the findings of this study are available from the corresponding author, upon reasonable request.

Acknowledgments: The authors thank the Universidad de Cartagena for the support to develop this research, laboratories, software, and time of the research team.

Conflicts of Interest: The authors declare no conflict of interest.

References

1. Kulbir, S.; Abdullahi, W.S.; Chhotu, R. Removal of Heavy Metals by Adsorption using Agricultural based Residue: A Review. *Res. J. Chem. Environ.* **2018**, *22*, 65–74.
2. De Gisi, S.; Lofrano, G.; Grassi, M.; Notarnicola, M. Characteristics and adsorption capacities of low-cost sorbents for wastewater treatment: A review. *Sustain. Mater. Technol.* **2016**, *9*, 10–40. [[CrossRef](#)]
3. Villabona-Ortiz, A.; De Cartagena, U.; Tejada-Tovar, C.N.; Ortega-Toro, R. Modelling of the Adsorption Kinetics Of Chromium (VI) Using Waste Biomaterials. *Rev. Mex. Ing. Química* **2020**, *19*, 401–408. [[CrossRef](#)]
4. Corral-Escárcega, M.C.; Ruiz-Gutiérrez, M.G.; Quintero-Ramos, A.; Meléndez-Pizarro, C.O.; Lardizabal-Gutiérrez, D.; Campos-Venegas, K. Use of biomass-derived from pecan nut husks (*Carya illinoensis*) for chromium removal from aqueous solutions. column modeling and adsorption kinetics studies. *Rev. Mex. Ing. Quim.* **2017**, *16*, 939–953.
5. Manjuladevi, M.; Anitha, R.; Manonmani, S. Kinetic study on adsorption of Cr(VI), Ni(II), Cd(II) and Pb(II) ions from aqueous solutions using activated carbon prepared from Cucumis melo peel. *Appl. Water Sci.* **2018**, *8*, 36. [[CrossRef](#)]
6. Chowdhury, Z.; Zain, S.M.; Rashid, A.; Rafique, R.F.; Khalid, K. Breakthrough Curve Analysis for Column Dynamics Sorption of Mn(II) Ions from Wastewater by Using Mangostana garcinia Peel-Based Granular-Activated Carbon. *J. Chem.* **2013**, *2013*, 1–8. [[CrossRef](#)]
7. Bhanvase, B.A.; Ugwekar, R.P.; Mankar, R.B. *Novel Water Treatment and Separation Methods: Simulation of Chemical Processes*; CRC Press: Boca Raton, FL, USA, 2017.
8. Sahu, O.; Singh, N. Significance of bioadsorption process on textile industry wastewater. In *The Impact and Prospects of Green Chemistry for Textile Technology*; Woodhead Publishing: Sawston, UK, 2019; pp. 367–416.
9. Hu, Q.; Xu, L.; Fu, K.; Zhu, F.; Yang, T.; Yang, T.; Luo, J.; Wu, M.; Yu, D. Ultrastable MOF-based foams for versatile applications. *Nano Res.* **2021**, 1–10. [[CrossRef](#)]
10. Qian, J.; Gao, X.; Pan, B. Nanoconfinement-Mediated Water Treatment: From Fundamental to Application. *Environ. Sci. Technol.* **2020**, *54*, 8509–8526. [[CrossRef](#)]
11. Elabbas, S.; Ouazzani, N.; Mandi, L.; Berrekhis, F.; Perdicakis, M.; Pontvianne, S.; Pons, M.-N.; Lapique, F.; Leclerc, J.-P. Treatment of highly concentrated tannery wastewater using electrocoagulation: Influence of the quality of aluminium used for the electrode. *J. Hazard. Mater.* **2016**, *319*, 69–77. [[CrossRef](#)]
12. Cherdchoo, W.; Nithetham, S.; Charoenpanich, J. Removal of Cr(VI) from synthetic wastewater by adsorption onto coffee ground and mixed waste tea. *Chemosphere* **2019**, *221*, 758–767. [[CrossRef](#)]
13. Bharathi, K.S.; Ramesh, S.P.T. Fixed-bed column studies on biosorption of crystal violet from aqueous solution by *Citrullus lanatus* rind and *Cyperus rotundus*. *Appl. Water Sci.* **2013**, *3*, 673–687. [[CrossRef](#)]
14. Jafari, S.A.; Jamali, A. Continuous cadmium removal from aqueous solutions by seaweed in a packed-bed column under consecutive sorption-desorption cycles. *Korean J. Chem. Eng.* **2016**, *33*, 1296–1304. [[CrossRef](#)]
15. Haroon, H.; Ashfaq, T.; Gardazi, S.M.H.; Sherazi, T.A.; Ali, M.; Rashid, N.; Bilal, M. Equilibrium kinetic and thermodynamic studies of Cr(VI) adsorption onto a novel adsorbent of *Eucalyptus camaldulensis* waste: Batch and column reactors. *Korean J. Chem. Eng.* **2016**, *33*, 2898–2907. [[CrossRef](#)]

16. Nordin, N.; Asmadi, N.A.A.; Manikam, M.K.; Halim, A.A.; Hanafiah, M.M.; Hurairah, S.N. Removal of Hexavalent Chromium from Aqueous Solution by Adsorption on Palm Oil Fuel Ash (POFA). *J. Geosci. Environ. Prot.* **2020**, *08*, 112–127. [[CrossRef](#)]
17. Villabona-Ortiz, A.; Tejada-Tovar, C.; Ruiz-Paternina, E.; Frías-González, J.D.; Blanco-García, G.D. Optimization of the Effect of Temperature and Bed Height on Cr (VI) Bioadsorption in Continuous System. *Rev. Fac. Ing.* **2020**, *29*, e10477. [[CrossRef](#)]
18. Haq, A.U.; Saeed, M.; Anjum, S.; Bokhari, T.H.; Usman, M.; Tubbsum, S. Evaluation of Sorption Mechanism of Pb (II) and Ni (II) onto Pea (*Pisum sativum*) Peels. *J. Oleo Sci.* **2017**, *66*, 735–743. [[CrossRef](#)]
19. Mohammadpour, E.; Yaftian, M.R.; Zamani, A.; Gharbani, P. Optimization of Continuous Flow Adsorption of Heavy Metal Ions on Continuous System Column by Peganum Harmala Seeds. *Arch. Hyg. Sci.* **2017**, *6*, 32–38. [[CrossRef](#)]
20. Borna, M.O.; Pirsaeheb, M.; Niri, M.V.; Mashizie, R.K.; Kakavandi, B.; Zare, M.R.; Asadi, A. Batch and column studies for the adsorption of chromium(VI) on low-cost Hibiscus Cannabinus kenaf, a green adsorbent. *J. Taiwan Inst. Chem. Eng.* **2016**, *68*, 80–89. [[CrossRef](#)]
21. Abdolali, A.; Ngo, H.H.; Guo, W.; Zhou, J.L.; Zhang, J.; Liang, S.; Chang, S.W.; Nguyen, D.D.; Liu, Y. Application of a breakthrough biosorbent for removing heavy metals from synthetic and real wastewaters in a lab-scale continuous fixed-bed column. *Bioresour. Technol.* **2017**, *229*, 78–87. [[CrossRef](#)]
22. Ruiz-Paternina, E.B.; Villabona-Ortiz, A.; Tejada-Tovar, C.; Ortega-Toro, R. Thermodynamic Study of the Removal of Nickel and Chromium in Aqueous Solution using Adsorbents of Agro-Industrial Origin. *Inf. Tecnol.* **2019**, *30*, 3–10. [[CrossRef](#)]
23. Naik, R.M.; Ratan, S.; Singh, I. Use of orange peel as an adsorbent for the removal of Cr (VI) from its aqueous solution. *Indian J. Chem. Technol.* **2018**, *25*, 300–305.
24. Abiazim, C.V.; Williams, A.B.; Inegbenebor, A.I.; Onwordi, C.T.; Ehi-Eromosele, C.O.; Petrik, L.F. Adsorption of lead ion from aqueous solution onto cellulose nanocrystal from cassava peel. *J. Phys. Conf. Ser.* **2019**, *1299*, 012122. [[CrossRef](#)]
25. Tejada-Tovar, C.; Ruiz-Paternina, E.; Gallo-Mercado, J.; Moscote-Bohorquez, J. Evaluation of the biosorption with african palm bagasse for the removal of Pb (II) in solution. *Rev. Prospect.* **2015**, *13*, 59–67.
26. Tejada-Tovar, C.; Gonzalez-Delgado, A.D.; Villabona-Ortiz, A. Characterization of Residual Biomasses and Its Application for the Removal of Lead Ions from Aqueous Solution. *Appl. Sci.* **2019**, *9*, 4486. [[CrossRef](#)]
27. Asuquo, E.D.; Martin, A.D. Sorption of cadmium (II) ion from aqueous solution onto sweet potato (*Ipomoea batatas* L.) peel adsorbent: Characterisation, kinetic and isotherm studies. *J. Environ. Chem. Eng.* **2016**, *4*, 4207–4228. [[CrossRef](#)]
28. Manirethan, V.; Gupta, N.; Balakrishnan, R.M.; Raval, K. Batch and continuous studies on the removal of heavy metals from aqueous solution using biosynthesised melanin-coated PVDF membranes. *Environ. Sci. Pollut. Res.* **2019**, *27*, 24723–24737. [[CrossRef](#)]
29. Rinaldi, R.; Yasdi, Y.; Hutagalung, W.L.C. Removal of Ni (II) and Cu (II) ions from aqueous solution using rambutan fruit peels (*Nephelium lappaceum* L.) as adsorbent. *AIP Conf. Proc.* **2018**, *2026*, 020098. [[CrossRef](#)]
30. Cai, J.; He, Y.; Yu, X.; Banks, S.; Yang, Y.; Zhang, X.; Yu, Y.; Liu, R.; Bridgwater, T. Review of physicochemical properties and analytical characterization of lignocellulosic biomass. *Renew. Sustain. Energy Rev.* **2017**, *76*, 309–322. [[CrossRef](#)]
31. Mahdi, Z.; Yu, Q.J.; El Hanandeh, A. Investigation of the kinetics and mechanisms of nickel and copper ions adsorption from aqueous solutions by date seed derived biochar. *J. Environ. Chem. Eng.* **2018**, *6*, 1171–1181. [[CrossRef](#)]
32. Wu, Y.; Fan, Y.; Zhang, M.; Ming, Z.; Yang, S.; Arkin, A.; Fang, P. Functionalized agricultural biomass as a low-cost adsorbent: Utilization of rice straw incorporated with amine groups for the adsorption of Cr(VI) and Ni(II) from single and binary systems. *Biochem. Eng. J.* **2016**, *105*, 27–35. [[CrossRef](#)]
33. Dai, Y.; Sun, Q.; Wang, W.; Lu, L.; Liu, M.; Li, J.; Yang, S.; Sun, Y.; Zhang, K.; Xu, J.; et al. Utilizations of agricultural waste as adsorbent for the removal of contaminants: A review. *Chemosphere* **2018**, *211*, 235–253. [[CrossRef](#)]
34. Tejada-Tovar, C.; Villabona, A.; Cabarcas, A.; Benitez, C.; Acevedo, D. Optimization of variables in fixed-bed column using the response surface methodology. *Contemp. Eng. Sci.* **2018**, *11*, 1121–1133. [[CrossRef](#)]
35. Labied, R.; Benturki, O.; Hamitouche, A.-E.; Donnot, A. Adsorption of hexavalent chromium by activated carbon obtained from a waste lignocellulosic material (*Ziziphus jujuba* cores): Kinetic, equilibrium, and thermodynamic study. *Adsorpt. Sci. Technol.* **2018**, *36*, 1066–1099. [[CrossRef](#)]
36. Srivastava, S.; Agrawal, S.B.; Mondal, M.K. Fixed bed column adsorption of Cr(VI) from aqueous solution using nanosorbents derived from magnetite impregnated Phaseolus vulgaris husk. *Environ. Prog. Sustain. Energy* **2019**, *38*, S68–S76. [[CrossRef](#)]
37. Deng, Y.; Huang, S.; Laird, D.A.; Wang, X.; Dong, C. Quantitative mechanisms of cadmium adsorption on rice straw- and swine manure-derived biochars. *Environ. Sci. Pollut. Res.* **2018**, *25*, 32418–32432. [[CrossRef](#)] [[PubMed](#)]
38. Deng, Y.; Huang, S.; Dong, C.; Meng, Z.; Wang, X. Competitive adsorption behaviour and mechanisms of cadmium, nickel and ammonium from aqueous solution by fresh and ageing rice straw biochars. *Bioresour. Technol.* **2020**, *303*, 122853. [[CrossRef](#)] [[PubMed](#)]
39. Kuppusamy, S.; Thavamani, P.; Megharaj, M.; Venkateswarlu, K.; Lee, Y.B.; Naidu, R. Oak (*Quercus robur*) Acorn Peel as a Low-Cost Adsorbent for Hexavalent Chromium Removal from Aquatic Ecosystems and Industrial Effluents. *Water Air Soil Pollut.* **2016**, *227*, 62. [[CrossRef](#)]
40. Medellín-Castillo, N. Biosorption of lead (II) in aqueous solution onto residues of natural fibers from the ixtle industry (*Agave lechuguilla* torr. and *Yucca carnerosana* (trel.) Mckelvey). *Rev. Int. Contam. Ambient.* **2017**, *33*, 269–280. [[CrossRef](#)]
41. Rodríguez Narvaez, O.M.; Peralta-Hernandez, J.M.; Goonetilleke, A.; Bandala, E.R. Treatment technologies for emerging contaminants in water: A review. *Chem. Eng. J.* **2017**, *323*, 361–380. [[CrossRef](#)]

42. Chen, Y.; An, D.; Sun, S.; Gao, J.; Qian, L. Reduction and Removal of Chromium VI in Water by Powdered Activated Carbon. *Materials* **2018**, *11*, 269. [[CrossRef](#)]
43. Basu, H.; Saha, S.; Mahadevan, I.A.; Pimple, M.V.; Singhal, R.K. Humic acid coated cellulose derived from rice husk: A novel biosorbent for the removal of Ni and Cr. *J. Water Process Eng.* **2019**, *32*, 100892. [[CrossRef](#)]
44. Ranasinghe, S.; Navaratne, A.; Priyantha, N. Enhancement of adsorption characteristics of Cr(III) and Ni(II) by surface modification of jackfruit peel biosorbent. *J. Environ. Chem. Eng.* **2018**, *6*, 5670–5682. [[CrossRef](#)]
45. Akpomie, K.G.; Eluke, L.O.; Ajiwe, V.I.E.; Alisa, C.O. Attenuation kinetics and desorption performance of *artocarpus altilis* seed husk for Co (II), Pb (II) And Zn (II) Ions. *Iran. J. Chem. Chem. Eng.* **2018**, *37*, 171–186.
46. Tejada-Tovar, C.; Herrera-Barros, A.; Ruiz-Paternina, E. Utilization of Biosorbents for Nickel and Lead Removal in Binary Systems. *Cienc. Desarro.* **2016**, *7*, 31–36. [[CrossRef](#)]
47. Oguz, E.; Ersoy, M. Biosorption of cobalt(II) with sunflower biomass from aqueous solutions in a fixed bed column and neural networks modelling. *Ecotoxicol. Environ. Saf.* **2014**, *99*, 54–60. [[CrossRef](#)]
48. Mishra, A.; Tripathi, B.D.; Rai, A.K. Packed-bed column biosorption of chromium(VI) and nickel(II) onto Fenton modified *Hydrilla verticillata* dried biomass. *Ecotoxicol. Environ. Saf.* **2016**, *132*, 420–428. [[CrossRef](#)]
49. Xavier, A.L.P.; Adarme, O.F.H.; Furtado, L.M.; Ferreira, G.M.D.; da Silva, L.H.M.; Gil, L.F.; Gurgel, L.V.A. Modeling adsorption of copper(II), cobalt(II) and nickel(II) metal ions from aqueous solution onto a new carboxylated sugarcane bagasse. Part II: Optimization of monocomponent fixed-bed column adsorption. *J. Colloid Interface Sci.* **2018**, *516*, 431–445. [[CrossRef](#)]
50. Banerjee, M.; Bar, N.; Basu, R.K.; Das, S.K. Removal of Cr(VI) from Its Aqueous Solution Using Green Adsorbent Pistachio Shell: A Fixed Bed Column Study and GA-ANN Modeling. *Water Conserv. Sci. Eng.* **2018**, *3*, 19–31. [[CrossRef](#)]
51. Tejada-Tovar, C.; Gallo-Mercado, J.; Moscote, J.; Villabona-Ortíz, A.; Acevedo-Correra, D. Competitive adsorption of lead and nickel on yam husk and palm bagasse in continuous system. *Rev. Biotechnol. Sect. Agropecu. Agroind.* **2018**, *16*, 52–61. [[CrossRef](#)]
52. Pradhan, P.; Arora, A.; Mahajani, S.M. Pilot scale evaluation of fuel pellets production from garden waste biomass. *Energy Sustain. Dev.* **2018**, *43*, 1–14. [[CrossRef](#)]
53. Amro, A.N.; Abhary, M.K.; Shaikh, M.M.; Ali, S. Removal of Lead and Cadmium Ions from Aqueous Solution by Adsorption on a Low-Cost Phragmites Biomass. *Processes* **2019**, *7*, 406. [[CrossRef](#)]
54. Blanes, P.S.; Bordoni, M.E.; González, J.C.; García, S.I.; Atria, A.M.; Sala, L.F.; Bellú, S.E. Application of soy hull biomass in removal of Cr(VI) from contaminated waters. Kinetic, thermodynamic and continuous sorption studies. *J. Environ. Chem. Eng.* **2016**, *4*, 516–526. [[CrossRef](#)]
55. Shahnaz, T.; Padmanaban, V.C.; Narayanasamy, S. Surface modification of nanocellulose using polypyrrole for the adsorptive removal of Congo red dye and chromium in binary mixture. *Int. J. Biol. Macromol.* **2020**, *151*, 322–332. [[CrossRef](#)] [[PubMed](#)]
56. Muhammad, A.; Shah, A.U.H.A.; Bilal, S. Effective Adsorption of Hexavalent Chromium and Divalent Nickel Ions from Water through Polyaniline, Iron Oxide, and Their Composites. *Appl. Sci.* **2020**, *10*, 2882. [[CrossRef](#)]